SIAM J. SCI. COMPUT.
Vol. 31, No. 3, pp. 1603–1627

TWO-LAYER SHALLOW WATER SYSTEM: A RELAXATION APPROACH*

RÉMI ABGRALL† AND SMADAR KARNI‡

Abstract. The two-layer shallow water system is an averaged flow model. It forms a nonconservative system which is only conditionally hyperbolic. The coupling between the layers, due to the hydrostatic pressure assumption, does not provide explicit access to the system eigenstructure, which is inconvenient for Riemann solution based numerical schemes. We consider a relaxation approach which offers greater decoupling and accessible eigenstructure. The stability of the model is discussed. Numerical results are shown for unsteady flows as well as for smooth and nonsmooth steady flows.

Key words. hyperbolic conservation laws, balance laws, shallow water equations, relaxation schemes

AMS subject classifications. 76M12, 35L65, 76N15, 76B70

DOI. 10.1137/06067167X

1. Introduction.

1.1. Preliminaries. The shallow water equations are commonly used to describe flows that are nearly horizontal. They can be obtained from the Euler equations by vertical averaging across the layer depth. The layers are distinguished by different densities ρ_1 and ρ_2, for example, due to different water salinity, with the lighter fluid placed on top of the heavier one, $\rho_2/\rho_1 = r \leq 1$. For modelling stratified flows, the regime $r \approx 1$ is of particular interest. The model is given by

$$
\begin{aligned}
&\frac{\partial}{\partial t}(\rho_1 h_1) + \frac{\partial}{\partial x}(\rho_1 h_1 u_1) = 0,\\
&\frac{\partial}{\partial t}(\rho_1 h_1 u_1) + \frac{\partial}{\partial x}\left(\rho_1 h_1 u_1^2 + g\rho_1 \frac{h_1^2}{2} + g\rho_2 h_1 h_2\right) = \rho_2 g h_2 \frac{\partial h_1}{\partial x} - \rho_1 g h_1 B'(x),\\
&\frac{\partial}{\partial t}(\rho_2 h_2) + \frac{\partial}{\partial x}(\rho_2 h_2 u_2) = 0,\\
&\frac{\partial}{\partial t}(\rho_2 h_2 u_2) + \frac{\partial}{\partial x}\left(\rho_2 h_2 u_2^2 + g\rho_2 \frac{h_2^2}{2}\right) = -\rho_2 g h_2 \frac{\partial h_1}{\partial x} - \rho_2 g h_2 B'(x),
\end{aligned}
\tag{1}
$$

with h_i and u_i denoting the respective layer depth and (averaged) velocity and $B(x)$ denoting the bottom elevation. The notation and setup for the two-layer system is illustrated in Figure 1. The system contains source terms due to bottom topography and nonconservative products describing momentum exchange between the layers. The latter cancel upon summation of the momenta equations, revealing the basic un-

*Received by the editors October 6, 2006; accepted for publication (in revised form) August 28, 2008; published electronically February 27, 2009. This work was supported in part by NSF award DMS 0609766.

http://www.siam.org/journals/sisc/31-3/67167.html

†University of Bordeaux, INRIA, and Institut Universitaire de France, Mathématiques Appliquées, Projet Scallaplix, 351 Cours de la Libération, 33 405 Talence Cedex, France (remi.abgrall@math.u-bordeaux1.fr).

‡Department of Mathematics, University of Michigan, Ann Arbor, MI 48109-1043 (karni@umich.edu).

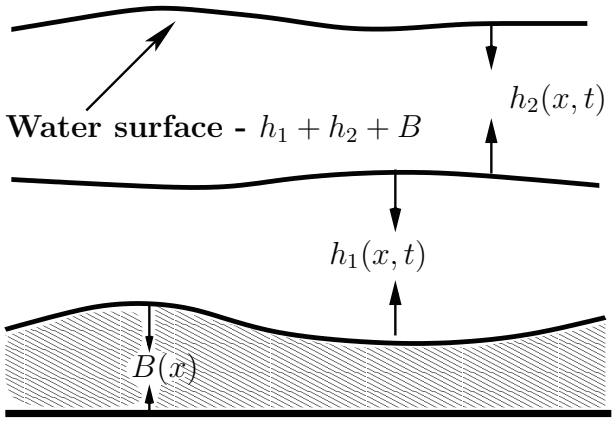

FIG. 1. *Two-layer shallow water model. Schematic.*

derlying momentum conservation. Yet, their presence has major consequences for the analysis of solutions and for their numerical computations; both rely on conservation in order to extend solutions beyond the time of discontinuity formation.

Following [1], the nonconservative product is defined by means of a path that connects the left and right states W_L and W_R, respectively, yielding jump conditions that are path dependent (see also [2]). The definition of the path is a crucial point and ideally should be dictated by the underlying physics. The shallow water system, being a layer-averaged flow model, does not offer a clear definition of a path. In the absence of a clear definition of a path, numerous choices may be made, all of which have an inherent level of arbitrariness in the resulting weak solutions. In the context of multiphase flow models, for example, in [3] the path is defined as the travelling wave that is the solution of a viscous regularization of the equation and in [4] the Volpert path is chosen (i.e., a straight line in the state space). In [5, 6], upwind schemes for the two-layer shallow water system were derived using the Volpert path. The work was generalized to channel flows in irregular geometries in [7, 8]. Other works on multilayer shallow systems include [9, 10]. See also [11] for a discussion on numerical schemes for nonconservative hyperbolic system and [12] for recent advances on numerical methods for hyperbolic systems and source term treatment.

1.2. The model. Using $W = (\rho_1 h_1, \rho_1 h_1 u_1, \rho_2 h_2, \rho_2 h_2 u_2)^T$ and $S = (0, -\rho_1 g h_1 B', 0, -\rho_2 g h_2 B')^T$ to denote the solution vector and the vector containing the geometric source due to bottom topography, respectively, the system may be written in the quasilinear form

$$W_t + A(W)W_x = S(x, W),$$

with

$$A(W) = \begin{pmatrix} 0 & 1 & 0 & 0 \\ gh_1 - u_1^2 & 2u_1 & gh_1 & 0 \\ 0 & 0 & 0 & 1 \\ rgh_2 & 0 & gh_2 - u_2^2 & 2u_2 \end{pmatrix}, \tag{2}$$

where the coefficient matrix $A(W)$ in (2) contains flux gradient terms as well as the nonconservative products.

The characteristic polynomial for the two-layer system is given by

$$\big((\lambda-u_1)^2-gh_1\big)\big((\lambda-u_2)^2-gh_2\big)=rg^2h_1h_2, \tag{3}$$

providing no simple analytic expression for the eigenvalues. First order expansions in u_2-u_1 give approximate expressions for the eigenvalues [13, 14]

$$\begin{aligned}\lambda^{\pm}_{ext}&=U_m\pm\sqrt{g(h_1+h_2)},\\ \lambda^{\pm}_{int}&=U_c\pm\sqrt{g'\frac{h_1h_2}{h_1+h_2}\left[1-\frac{(u_1-u_2)^2}{g'(h_1+h_2)}\right]},\end{aligned} \tag{4}$$

where

$$U_m=\frac{h_1u_1+h_2u_2}{h_1+h_2},\qquad U_c=\frac{h_1u_2+h_2u_1}{h_1+h_2},$$

and $g'=(1-r)g$ is the *reduced gravity*. The expressions for the approximate eigenvalues suggest that the system (1) is only conditionally hyperbolic, provided

$$\big(u_1-u_2\big)^2<g'\big(h_1+h_2\big). \tag{5}$$

Violation of condition (5) is linked to Kelvin–Helmholtz interfacial instability associated with shear flows, for which the vertically averaged shallow water model (1) is not suitable. We note, however, that condition (5) should be taken as an indication only. It is not sufficient to ensure hyperbolicity, nor is it necessary.

Estimation of eigenvalues.

Internal eigenvalues. The eigenvalues of system (1) may be estimated using the *single-layer* eigenvalues

$$\sigma_i^{\pm}=u_i\pm c_i,\qquad c_i=\sqrt{gh_i}.$$

We use $\sigma_i^{\pm}$ to write the characteristic polynomial (3) of the two-layer system as

$$P(\lambda)=\prod_{\sigma_i^{\pm}}(\lambda-\sigma_i^{\pm})-rc_1^2c_2^2,$$

and one can readily see that

$$P(\sigma_i^{\pm})=-rc_1^2c_2^2.$$

Using elementary calculus arguments, one can see that the derivative of P has three real zeros so that P has three extremas. Hence the generic form of P is displayed in Figure 2. In case (a), P has four real zeros; in case (b), P has two real roots and two complex roots.

Let us denote by $\alpha^{\pm}$ ($\alpha^-\le\alpha^+$) the two real roots that always exist and by $\beta^{\pm}$ the two others so that when all four roots are real

$$\alpha^-\le\beta^-\le\beta^+\le\alpha^+.$$

Similarily, we order the set $\{\sigma_i^{\pm}\}$ by increasing order and denote the ordered set by

$$\{\sigma_1\le\sigma_2\le\sigma_3\le\sigma_4\}.$$

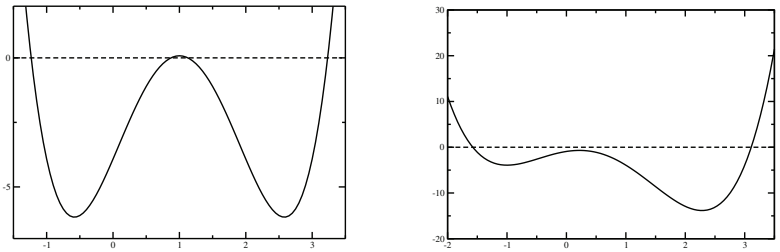

(a) (b)

FIG. 2. *The two possible configurations* (a) *four real eigenvalues,* (b) *two real eigenvalues.*

Using simple calculus arguments that rely on the sign of $P'(\lambda)$, we see that

$$\alpha^- \leq \sigma_1 \leq \sigma_2 \leq \beta^- \leq \beta^+ \leq \sigma_3 \leq \sigma_4 \leq \alpha^+$$

so that

$$|\beta^\pm| \leq \max\{|\sigma_2|, |\sigma_3|\}.$$

External eigenvalues. We rewrite the characteristic polynomial

$$P(\lambda) = \big((\lambda - u_1)^2 - c_1^2\big)\big((\lambda - u_2)^2 - c_2^2\big) - rc_1^2c_2^2$$

and consider $\lambda_1^\pm$ the roots of

$$(\lambda - u_1)^2 - c_1^2 = \sqrt{r}c_1^2$$

and $\nu_1^\pm$ the roots of

$$(\lambda - u_2)^2 - c_2^2 = \sqrt{r}c_2^2.$$

We define $\alpha = \max(\lambda_1^\pm, \nu_1^\pm)$ and claim that $P(\alpha) \geq 0$. To fix notation, we assume for the sake of simplicity that $\alpha = \lambda_1^+$. Then

$$\begin{aligned} P(\alpha) &= \big((\lambda_1^+ - u_1)^2 - c_1^2\big)\big((\lambda_1^+ - u_2)^2 - c_2^2\big) - rc_1^2c_2^2 \\ &= \sqrt{r}c_1^2\big((\lambda_1^+ - u_2)^2 - c_2^2\big) - rc_1^2c_2^2 \\ &= \sqrt{r}c_1^2\left((\lambda_1^+ - u_2)^2 - c_2^2 - \sqrt{r}c_2^2\right) \\ &\geq 0 \end{aligned}$$

because $\sqrt{r}c_1^2 \geq 0$ and $(\lambda_1^+ - u_2)^2 - c_2^2 - \sqrt{r}c_2^2 \geq 0$. By definition, α is larger than either of the roots of this quadratic concave polynomial; hence λ does not belong to the interval defined by its root. The quadratic polynomial evaluated at α is therefore positive.

Then $\alpha \geq u_1 + c_1$ and $\alpha \geq u_2 + c_2$ in the general case because we have

$$\begin{aligned} \alpha \geq \lambda_1^+ = u_1 + \sqrt{1 + \sqrt{r}}c_1 \geq u_1 + c_1, \\ \alpha \geq \nu_1^+ = u_2 + \sqrt{1 + \sqrt{r}}c_2 \geq u_2 + c_2 \end{aligned}$$

so that α must be greater than the largest root of P. Similarly, we have $\beta = \min(\lambda_1^\pm, \nu_1^\pm)$ is smaller than all of the roots of P.

Other bounds may also be found, for example, by using the roots of

$$(\lambda - u_1)^2 - c_1^2 = \sqrt{r}c_2^2 \qquad \text{and} \qquad (\lambda - u_2)^2 - c_2^2 = \sqrt{r}c_1^2,$$

namely,

$$u_1 \pm \sqrt{c_1^2 + \sqrt{r}c_2^2}, \qquad u_2 \pm \sqrt{c_2^2 + \sqrt{r}c_1^2}.$$

The implementation of the numerical scheme via the relaxation model (7) requires an estimation of the eigenvalues of system (1). In the numerical experiments, we have estimated the internal eigenvalues by $\max\{|u_1| + c_1, |u_2| + c_2\}$ and $\max\left\{|u_1| + \sqrt{(1+\sqrt{r})}c_1, |u_2| + \sqrt{(1+\sqrt{r})}c_2\right\}$ to bound the external eigenvalues.

1.3. Entropy function. System (1) is endowed with an entropy function, given by the total energy in the layers

$$\mathcal{H} = \rho_1 h_1 \frac{u_1^2}{2} + \rho_2 h_2 \frac{u_2^2}{2} + \rho_1 g \frac{h_1^2}{2} + \rho_2 g \frac{h_2^2}{2} + \rho_2 g h_1 h_2$$

in analogy with the single-layer case. The entropy flux $\mathcal{G}$ is defined by

$$\begin{aligned}\mathcal{G} =& \frac{1}{2}\big(\rho_1 h_1 u_1^3 + \rho_2 h_2 u_2^3\big) \\ &+ g\big(\rho_1 h_1^2 u_1 + \rho_2 h_1 h_2 u_1 + \rho_2 h_1 h_2 u_2 + \rho_2 h_2^2 u_2\big)\end{aligned}$$

so that, for smooth solutions,

$$\frac{\partial \mathcal{H}}{\partial t} + \operatorname{div}(\mathcal{G}) = 0.$$

An easy calculation shows that $\mathcal{H}$ is a convex function in the "conserved" variables provided that $\rho_2 \le \rho_1$, as is the case here. We note that the existence of a convex entropy function is not in contradiction with the fact that system (1) is only conditionally hyperbolic, because system (1) is not set in conservation form, as required for the classical proof to hold; see [15] for more details.

1.4. Steady state solutions. Smooth steady state solutions of (1) satisfy

$$\begin{aligned} Q_1 &= h_1 u_1, & E_1 &= \tfrac{1}{2}u_1^2 + g\big(h_1 + B\big) + r g h_2, \\ Q_2 &= h_2 u_2, & E_2 &= \tfrac{1}{2}u_2^2 + g\big(h_1 + h_2 + B\big), \end{aligned} \tag{6}$$

where Q_1, Q_2, E_1, and E_2 are constants representing the (specific) mass flow rate and energy, respectively, in the respective layers. Once these four parameters are specified, the smooth steady flow is completely determined, and system (6) may be solved by nonlinear root finding. The structure of smooth and nonsmooth steady shallow water flow bears great resemblance to steady flow in a converging-diverging channel, with the role of the *Mach number* in channel flow assumed by the *Froude number* in shallow water flow (see below). The two-layer case poses the additional (significant) complication that the governing equations are in nonconservation form. In a series of illuminating papers pointed out by [5], Armi and Farmer [16, 17, 18] have presented a theoretical study of the hydraulics of two flowing layers. This theory provides insight into the relevant range of parameters and their effect on the resulting flow and, for completeness, is briefly described in Appendix A. The theory is developed under the so-called *rigid-lid* assumption. Under the same assumption, we derive jump conditions valid across hydraulic jumps, also given in Appendix A.

2. A relaxation model. Violation of condition (5) is often associated with shear layer Kelvin–Helmholtz instabilities of the interface separating the two fluid layers. Even within the hyperbolic regime, the eigenstructure of (1) is given only implicitly, due to the form of nonlinear coupling between the layers. As a result, if the numerical method requires characteristic field decomposition (for example, Roe-type method), the eigenvalues need to be computed by numerical root finding and the corresponding eigenvectors by solving numerically a linear system (see [5, 7]). In the absence of analytic expressions for the eigenvectors, building desirable properties into the scheme, for example, accuracy near steady state, may be more difficult. In the present section, we propose a relaxation approach to address these issues.

We reexamine the coefficient matrix $A(W)$ in (2). We define two auxiliary variables $h_1^{'}$ and $h_2^{'}$ and propose the relaxation model

$$
\begin{aligned}
&\frac{\partial}{\partial t}(\rho_1 h_1) + \frac{\partial}{\partial x}(\rho_1 h_1 u_1) = 0,\\
&\frac{\partial}{\partial t}(\rho_1 h_1 u_1) + \frac{\partial}{\partial x}\left(\rho_1 h_1 u_1^2 + \rho_1 g\frac{h_1^2}{2} + \boxed{\rho_2 g h_1 h_2^{'}}\right) = \boxed{\rho_2 g h_2 \frac{\partial h_1^{'}}{\partial x}} - \rho_1 g h_1 B'(x),\\
&\frac{\partial}{\partial t}(\rho_2 h_2) + \frac{\partial}{\partial x}(\rho_2 h_2 u_2) = 0,\\
&\frac{\partial}{\partial t}(\rho_2 h_2 u_2) + \frac{\partial}{\partial x}\left(\rho_2 h_2 u_2^2 + \rho_2 g\frac{h_2^2}{2}\right) = -\boxed{\rho_2 g h_2 \frac{\partial h_1^{'}}{\partial x}} - \rho_2 g h_2 B'(x),\\
&\frac{\partial}{\partial t}h_1^{'} + U_1^*\frac{\partial}{\partial x}h_1^{'} = \frac{h_1^{'} - h_1}{\epsilon},\\
&\frac{\partial}{\partial t}h_2^{'} + U_2^*\frac{\partial}{\partial x}h_2^{'} = \frac{h_2^{'} - h_2}{\epsilon},
\end{aligned}
\tag{7}
$$

where ϵ is a relaxation parameter of $h_i^{'} \to h_i$ and U_i^* are propagation speeds associated with the auxialiary variables $h_i^{'}$, which are at our disposal. For convenience, we have identified the terms in the original system (1) that are affected by the introduction of the auxiliary variables.

The extended system (7) can be written in the quasi-linear form

$$W_t + A(W)W_x = S(x, W) + \frac{1}{\epsilon}R(W),$$

with

$$
\begin{aligned}
W &= \left(\rho_1 h_1,\ \rho_1 h_1 u_1,\ \rho_2 h_2,\ \rho_2 h_2 u_2,\ h_1^{'},\ h_2^{'}\right)^T,\\
S &= \left(0,\ -\rho_1 g h_1 B',\ 0,\ -\rho_2 g h_2 B',\ 0,\ 0\right)^T,\\
R &= \left(0,\ 0,\ 0,\ 0,\ h_1^{'} - h_1,\ h_2^{'} - h_2\right)^T,\\
A &= \begin{pmatrix}
0 & 1 & 0 & 0 & 0 & 0\\
c_1^2 - u_1^2 & 2u_1 & 0 & 0 & -\rho_2 g h_2 & \rho_2 g h_1\\
0 & 0 & 0 & 1 & 0 & 0\\
0 & 0 & c_2^2 - u_2^2 & 2u_2 & \rho_2 g h_2 & 0\\
0 & 0 & 0 & 0 & U_1^* & 0\\
0 & 0 & 0 & 0 & 0 & U_2^*
\end{pmatrix},
\end{aligned}
\tag{8}
$$

where for convenience we have introduced the "*sound speeds*"

$$c_1^2 = g h_1 + r g h_2^{'}, \qquad c_2^2 = g h_2.$$

The extended model "hyperbolizes" the system in the sense that it has eigenvalues that are always real given by

$$\lambda_{1,2} = u_1 \mp c_1 \ , \qquad \lambda_{3,4} = u_2 \mp c_2 \ , \qquad \lambda_5 = U_1^* \ , \qquad \lambda_6 = U_2^*, \tag{9}$$

and the matrix of right eigenvectors is

$$RR = \begin{pmatrix} 1 & 1 & 0 & 0 & a & c \\ u_1 - c_1 & u_1 + c_1 & 0 & 0 & U_1^* a & U_2^* c \\ 0 & 0 & 1 & 1 & b & 0 \\ 0 & 0 & u_2 - c_2 & u_2 + c_2 & U_1^* b & 0 \\ 0 & 0 & 0 & 0 & 1 & 0 \\ 0 & 0 & 0 & 0 & 0 & 1 \end{pmatrix}, \tag{10}$$

with

$$\begin{aligned} a &= \frac{\rho_2 g h_2^{'}}{c_1^2 - (u_1 - U_1^*)^2}, \\ b &= \frac{-\rho_2 g h_2}{c_2^2 - (u_2 - U_1^*)^2}, \\ c &= \frac{-\rho_2 g h_1}{c_1^2 - (u_1 - U_2^*)^2}. \end{aligned} \tag{11}$$

We note that we do not view the relaxation system as a means to get around the conditional hyperbolicity limitations of the two-layer shallow water system (1). Indeed, loss of hyperbolicity may indicate that the underlying model ceases to be valid, a feature that should not be suppressed. We view the relaxation system as a tool to decouple system (1) and provide a system which is equivalent in the limit $\epsilon \to 0$ and has easily accessible eigenstructure.

Our interest is in the behavior of the above relaxation system as $\epsilon \to 0$. We next establish that solutions to the perturbed system (7), in the limit $\epsilon \to 0$, recover solutions to (1) when projected back onto the original solution space and study its stability.

3. Stability.

3.1. Perturbation analysis. The analysis in this section follows Murrone and Guillard [19]. We denote by W_0 the equilibrium solution to (7), satisfying $R(W_0) = 0$, and seek solutions of the formal asymptotic form $W = W_0 + \epsilon W_1 + \epsilon^2 W_2 + \cdots$. Collecting zero order terms in ϵ gives

$$\frac{\partial W_0}{\partial t} + A(W_0)\frac{\partial W_0}{\partial x} = R'(W_0)W_1 + S(x, W_0). \tag{12}$$

The formal asymptotic limit of the extended system (7) as $\epsilon \to 0$ is governed by the structure of $R'(W)$:

$$R'(W) = \begin{pmatrix} 0 & 0 & 0 & 0 & 0 & 0 \\ 0 & 0 & 0 & 0 & 0 & 0 \\ 0 & 0 & 0 & 0 & 0 & 0 \\ 0 & 0 & 0 & 0 & 0 & 0 \\ 1/\rho_1 & 0 & 0 & 0 & -1 & 0 \\ 0 & 1/\rho_2 & 0 & 0 & 0 & -1 \end{pmatrix}, \tag{13}$$

whose kernel and range are spanned by

$$\begin{aligned}
\ker R'(W) &= \text{Span}\left\{\begin{pmatrix}\rho_1\\0\\0\\0\\1\\0\end{pmatrix},\ \begin{pmatrix}0\\\rho_2\\0\\0\\0\\1\end{pmatrix},\ \begin{pmatrix}0\\0\\1\\0\\0\\0\end{pmatrix},\ \begin{pmatrix}0\\0\\0\\1\\0\\0\end{pmatrix}\right\},\\
\text{range } R'(W) &= \text{Span}\left\{\begin{pmatrix}0\\0\\0\\0\\1\\0\end{pmatrix},\ \begin{pmatrix}0\\0\\0\\0\\0\\1\end{pmatrix}\right\}
\end{aligned} \tag{14}$$

forming, together, a basis for $\Re^6 = \ker R'(W) \oplus \text{range } R'(W) = \text{Span}\{r_k, k = 1, \cdots, 6\}$.

Let P be the projection along range $R'(W)$ onto $\ker R'(W)$ satisfying $PR'(W_0) \equiv 0$. Then

$$P\left(\frac{\partial W_0}{\partial t} + A(W_0)\frac{\partial W_0}{\partial x}\right) = P\Big(S(W_0) + R'(W_0)W_1\Big) = PS(W_0) \tag{15}$$

recovers the equilibrium system (1). Solutions $W \in \Re^6$ to (7) may be expressed in terms of $\{r_k\}$ defined above:

$$W = \sum_{k=1}^{6} \alpha_k r_k = \big(a,\ b,\ c,\ d,\ e,\ f\big)^T. \tag{16}$$

A simple calculation verifies that

$$PW = P\left(\sum_{k=1}^{6}\alpha_k r_k\right) = \left(\sum_{k=1}^{4}\alpha_k r_k\right) = \left(\underbrace{a,\ b,\ c,\ d}_{unchanged},\ a/\rho_1,\ b/\rho_2\right)^T, \tag{17}$$

which preserves the first four components of the solution vector and implies that the extended solution, restricted to its first four components, is also a solution of the equilibrium system (1).

3.2. Subcharacteristic condition and dissipativity. The preceding formal asymptotic analysis does not imply that the expansion is convergent. Stability of relaxation models in the limit $\epsilon \to 0$ is studied through the Chapman–Enskog expansion [20]. In the classical setup for stability analysis, the conservation law

$$\frac{\partial w}{\partial t} + \frac{\partial f(w)}{\partial x} = 0 \tag{18}$$

is approximated by the relaxation system

$$\frac{\partial w^\epsilon}{\partial t} + \frac{\partial v}{\partial x} = 0\ , \qquad \frac{\partial v}{\partial t} + a\frac{\partial w^\epsilon}{\partial x} = \frac{1}{\epsilon}\left(v - f(w^\epsilon)\right)$$

for some (positive) parameter a. In the limit $\epsilon \to 0$, $v = f(w)$ to leading order in ϵ, and the equilibrium conservation law is recovered. First order corrections yield the second order perturbed equation

$$\frac{\partial w^\epsilon}{\partial t} + \frac{\partial f(w^\epsilon)}{\partial x} = \epsilon \frac{\partial}{\partial x}\left\{ \left(a - f'(w^\epsilon)^2 \right) \frac{\partial w^\epsilon}{\partial x} \right\} \tag{19}$$

which is well-posed provided it is dissipative, that is, if

$$a - f'(w)^2 \geq 0 \tag{20}$$

or equivalently if

$$-\sqrt{a} \leq f'(w) \leq \sqrt{a}. \tag{21}$$

This is the so-called *subcharacteristic condition*. Under suitable assumptions, condition (21) implies convergence of the relaxation system (see, for example, [21, 22]; for a survey of more recent results on hyperbolic systems with relaxation, see also [23]). This condition may be interpreted as a *CFL-like* condition, requiring that the propagation speeds of the relaxation system (7) be no smaller than the propagation speeds of the equilibrium system (1).

System (7), however, does not fall into the above category of relaxation models. In particular, the relationship between the subcharacteristic condition and dissipativity of the perturbed system take a different form. Indeed, a standard Chapman–Enskog expansion of (15) up to terms of order ϵ gives

$$P\left(\frac{\partial W_0}{\partial t} + A(W_0)\frac{\partial W_0}{\partial x} \right) = P\left(S(W_0) + R'(W_0)W_1 \right) = PS(W_0) + \epsilon P \frac{\partial}{\partial x}\left(DP \frac{\partial W_0}{\partial x} \right), \tag{22}$$

with (see Appendix C)

$$D = \begin{pmatrix} 0 & 0 & 0 & 0 \\ 0 & \rho_2 g h_1 h_2 \dfrac{\partial u_1}{\partial x} & 0 & 0 \\ 0 & 0 & 0 & 0 \\ 0 & 0 & 0 & g\rho_2 h_2^2 \dfrac{\partial u_2}{\partial x} \end{pmatrix},$$

which is a matrix whose eigenvalues are not necessarily positive.

Furthermore, the relaxation system (7), as the subcharacteristic condition (21) suggests, is required to be able to support the stable propagation of waves of the underlying equilibrium system, and these waves may be travelling at speeds faster than its own. We adopt this loose CFL-like notion of stability and pursue further this point at the discrete (numerical) level. More specifically, we bound the speeds of the underlying equilibrium system and modify the numerical viscosity of the scheme so that it is stable up to those speed bounds. The details are given in section 5.

4. Numerical method. We solve (7) using a split-step method consisting of a propagation step followed by a relaxation step:

- *Propagation step.* Solve

$$\frac{\partial W}{\partial t} + A(W)\frac{\partial W}{\partial x} = S(x, W).$$

- *Relaxation step.* Solve

$$\frac{\partial W}{\partial t} = \frac{1}{\epsilon} R(W)$$

in the limit of instantaneous relaxation $\epsilon \to 0$. This step amounts to resetting the auxiliary variables to their relaxed values

$$h_1^{'} := h_1 \ , \qquad h_2^{'} := h_2.$$

4.1. Roe linearization. For the propagation step, we use a Roe-type method. The eigenvalues and eigenvectors of the relaxation system (7) are given in (9) and (10). In the absence of momentum exchange terms, the system is in conservation form and has a Roe linearization [24]. That is, there exists a Roe matrix $\overline{A}$ satisfying $\Delta F = \overline{A}\Delta W$. The averages are given by

$$\overline{h_1} = \frac{h_1^L + h_1^R}{2} \ , \qquad \overline{u_1} = \frac{\sqrt{h_1^L}u_1^L + \sqrt{h_1^R}u_1^R}{\sqrt{h_1^L} + \sqrt{h_1^R}},$$
$$\overline{h_2} = \frac{h_2^L + h_2^R}{2} \ , \qquad \overline{u_2} = \frac{\sqrt{h_2^L}u_2^L + \sqrt{h_2^R}u_2^R}{\sqrt{h_2^L} + \sqrt{h_2^R}}.$$

The geometrical source terms due to bottom topography are upwinded by projecting them onto the eigenvectors (10) of the coefficient matrix (see [25])

$$S = \sum_{k=1}^{6} \beta_k r_k.$$

The strengths of those projections are

$$\beta_1 = \frac{\rho_1 g h_1 B'(x)}{2c_1} = -\beta_2 \ , \qquad \beta_3 = \frac{\rho_2 g h_2 B'(x)}{2c_2} = -\beta_4 \ , \qquad \beta_5 = \beta_6 = 0 \ . \tag{23}$$

4.2. Steady states. Time changes in the solution arise if the flux gradient and the source terms are out of balance. Schemes that are able to recognize such a balance often give superior results when computing near steady state solutions. Perfectly recognizing such a balance is not always possible as it may place too many conditions with too few degrees of freedom to satisfy them. Typically, one aims at respecting steady states either exactly or to the order of the numerical approximation. One trivial steady state of (1) is the steady state of rest

$$u_1 = u_2 = 0 \ , \qquad h_1 + B = Const \ , \qquad h_2 = Const.$$

A straightforward calculation shows that if the source term S is approximated using

$$\overline{B'(x)} = \frac{\Delta B}{\Delta x}, \qquad \overline{h_1} = \frac{\left(h_1\right)_L + \left(h_1\right)_R}{2},$$

then the total fluctuation

$$\lambda_k \alpha_k - \Delta x \beta_k, \qquad k = 1, \ldots, 4,$$

vanishes identically for steady states of rest, resulting in zero change to the solution (more precisely, to the restriction of the solution to its first four components, which is all that is needed).

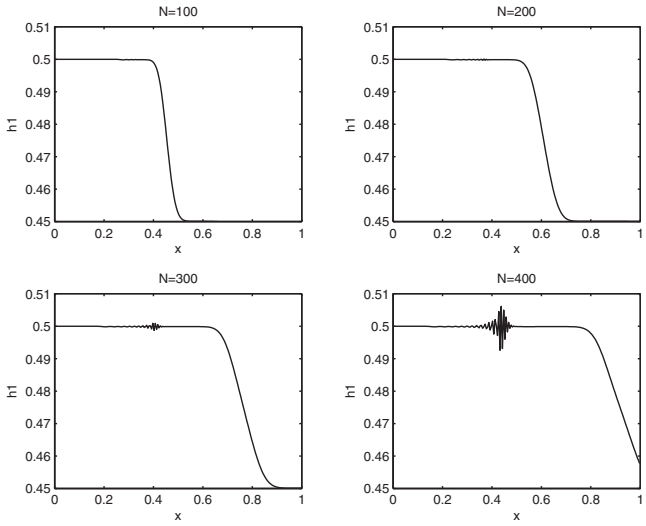

FIG. 3. *Interfacial instability. Relaxation model.*

5. Numerical results. The following examples use $g = 10$ and $r = 0.98$.

5.1. Time dependent example. This example is taken from [5]. The bottom topography is flat, $B(x) = 0$, and initial data is given by

$$\begin{array}{llll} (h_1)_L = 0.5, & (q_1)_L = 1.25, & (h_1)_R = 0.45, & (q_1)_R = 1.125, \\ (h_2)_L = 0.5, & (q_2)_L = 1.25, & (h_2)_R = 0.55, & (q_2)_R = 1.375. \end{array} \tag{24}$$

In [5] this example was used to illustrate that a layer-by-layer approach for the two-layer system is not suitable and may go unstable. We use this example to complete the stability discussion of the proposed relaxation scheme. The number of grid points is 200, and the CFL number is 0.7. The solution appears to consist of an interfacial wave moving to the right (see Figure 3). As the wave moves along, an instability develops, which rather quickly contaminates the solution and causes the solution to break down.

We recall that it is possible that the equilibrium system (1) produces faster waves than can be supported by the relaxation system (7). In this case, the numerical viscosity associated with the scheme may generate insufficient dissipation to stabilize the fast waves of the underlying equilibrium system (1) and may be responsible for triggering the instability observed in Figure 3.

For the upwind scheme, given here in the form of wave signals

$$\begin{aligned} A^+\Delta W &= \sum_k \frac{\lambda_k + |\lambda_k|}{2}\alpha_k r_k, \\ A^-\Delta W &= \sum_k \frac{\lambda_k - |\lambda_k|}{2}\alpha_k r_k, \end{aligned} \tag{25}$$

the amount of numerical viscosity is controlled by $|\lambda_k|$, and the method is stable for wave speeds up to $|\lambda_k|$. To stablize the method for possibly faster waves in the underlying equilibrium system, we propose to estimate those speeds and replace the

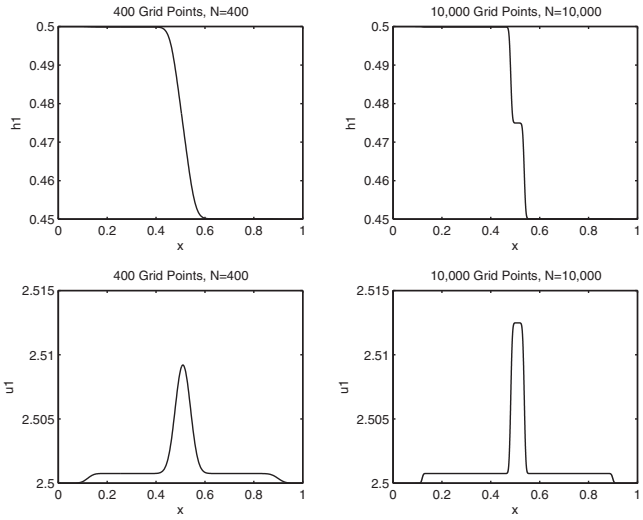

FIG. 4. *Interfacial instability. Relaxation model with "subcharacteristic" viscosity.*

expression for the numerical viscosity in (25) by

$$\left|\tilde{\lambda}_k\right| = \max\left\{\left|\lambda_k\right|,\ \left|\sigma_k\right|\right\}\ , \qquad k = 1, 2, 3, 4, \tag{26}$$

where σ_k are suitable bounds on the eigenvalues (3) of the original system and λ_k are the eigenvalues (9) of the relaxation system. In section 1.2, we used standard calculus arguments to provide such bounds. We showed that when the *exact* internal eigenvalues of system (1) are real, they may be bounded by $|\sigma| := \max(|s_2|, |s_3|)$, where s_k are the ordered set of the *single-layer* eigenvalues. The external wave speeds are always real. We provided bounds for the external wave too, although our experience is that not bounding the external wave speeds does not seem to trigger instabilities. See section 1.2.

Figure 4 shows the computation of the same problem (24), with the modified viscosity (26) using 400 grid points and CFL number 0.7. The computation is clearly stablized by the modified viscosity. Furthermore, a fine grid calculation, using 10,000 grid points, reveals that what appeared to be a single wave is, in fact, a four-wave structure, all clearly visible on the velocity plot.

The fact that an underlying unstable relaxation model may be stablized at the discrete level is not inconceivable. In Appendix D, we present numerical experiments investigating the intricate interplay between the parameter ϵ and the numerical parameters. We conclude from this quick study that the instability implied by the Chapman–Enskog expansion provides only a crude indication of the stability of the numerical solutions, and small parameters such as the grid size certainly play an important role in the final stability account.

5.2. Steady state solutions.

5.2.1. State of rest. Figure 5 shows two calculations in which the initial data corresponds to steady states of rest, with $u_1 = u_2 = 0$, $h_1 + B(x) = 1$, and $h_2 = 1$.

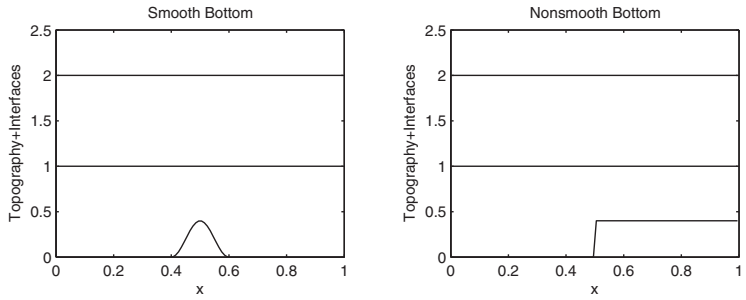

FIG. 5. *Steady state of rest. Smooth topography (left), nonsmooth topography (right).*

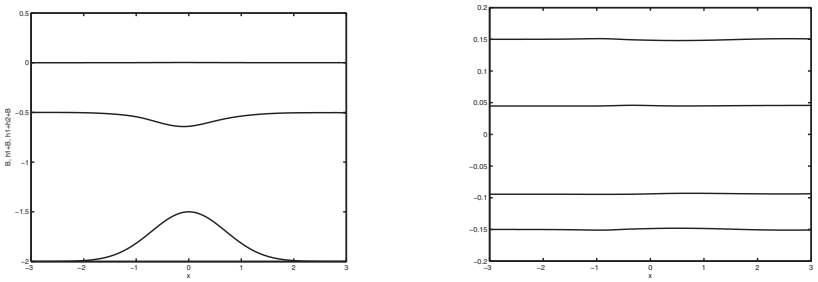

FIG. 6. *Smooth subcritical steady state. Interface and water surface (left), steady state flow constants $Q_{1,2}$ and $E_{1,2}$ (right).*

The left calculation is over smooth bottom topography

$$B(x) = \begin{cases} 0.2\left(\cos\pi\left(\dfrac{x-\frac{1}{2}}{0.1}\right)+1\right), & \left|x-\dfrac{1}{2}\right| \le 0.1, \\ 0, & \text{otherwise} \end{cases}$$

and the right is over a step function

$$B(x) = \begin{cases} 0, & x \le 0.5, \\ 0.4, & x > 0.5. \end{cases}$$

In both examples, the numerical method, as described in section 4.2, recognizes and respects the initial steady state of rest and the computed solution remains unchanged.

5.2.2. Smooth subcritical flow. In this example, taken from [5], the domain is set to $\big[-3,3\big]$, and the bottom topography is given by a smooth exponential

$$B(x) = \frac{1}{2}e^{-x^2} - 2.$$

We specify the flow rates $Q_1 = 0.15$ and $Q_2 = -0.15$ at inflow and the layer depths $h_1 = 1.5$ and $h_2 = 0.5$ at outflow. Note that inflow/outflow here means opposite sides for the respective layers. We have used a CFL number 0.6 and discretized the domain using various grids. The resulting steady flow, shown in Figure 6, remains subcritical and smooth. To a very good approximation, the top surface is horizontal, corresponding to a fixed total depth. As a measure of "steadiness," we also plot

the flow discharge and energy in the respective layers $Q_{1,2}$ and $E_{1,2}$. These flow parameters are constant for the exact steady solution and to a good agreement are constant in the computations. L_1 errors in q_1 are 5.16910^{-3}, 3.20810^{-3}, 1.77610^{-3}, and 9.37510^{-4} and in q_2 are 4.91410^{-3}, 3.12310^{-3}, 1.73310^{-3}, and 9.16710^{-4} on grids using 400, 800, 1,600, and 3,200 points, respectively, reflecting roughly first order convergence (see Figure 6 (right)).

5.2.3. Smooth transcritical flow. The next example corresponds to transcritical flows connecting two infinite reservoirs, accelerating smoothly from sub- to supercritical, reaching criticality right at the crest, $B'(x) = 0$. The example follows the one given in [8] and corresponds to the so-called *maximal flow* (see [18]). We note that steady rigid-lid solutions depend on Q_i^2 and as such make no distinction between layers flowing in the same direction (parallel flow) or in opposite direction (exchange flow), with the latter being more prone to shear layer instability. Both cases have been computed and are compared to the exact steady rigid-lid solution described in Appendix A (see also [18]).

Parallel flow. The domain is $-3 \le x \le 3$, and the bottom topography is give by

$$B(x) = \begin{cases} 0.125\left(\cos\dfrac{\pi}{2}x + 1\right)^2, & |x| \le 2, \\ 0, & \text{otherwise.} \end{cases}$$

The boundary conditions specify the flow rates at inflow and the depth of the layers at outflow and are given by

$$\begin{aligned} (Q_1)_{in} &= 0.09282893, & (H_1)_{out} &= 0.1616669, \\ (Q_2)_{in} &= 0.09282893, & (H_2)_{out} &= 1.3338331, \end{aligned}$$

with the two layers flowing in the same direction so that inflow is on the left and outflow is on the right. The initial condition for this calculation is a "smeared" jump

$$h_i(x) = \begin{cases} (H_i)_{in}, & -3 < x < -2, \\ 0.25\big((H_i)_{in}(2-x) + (H_i)_{out}(2+x)\big), & -2 \le x \le 2, \\ (H_i)_{out}, & 2 < x < 3. \end{cases}$$

In general, the steady state solution depends only on the boundary conditions and not on the initial data. Transcritical flows of this kind, however, may exhibit weak dependence on the initial data in that they need to be not "too far" from the steady solution in order to converge. The domain has been discretized using 501 grid points and a CFL number 0.6. Figure 7 shows very good agreement between the exact rigid-lid solution and the computed solution, with a slight discrepancy visible on the left of the topographical bump. We believe that this discrepancy is due to the fact that the exact solution is a rigid-lid solution, not an exact steady state solution of (1), so discrepencies are to be expected. The computed energies in the layers $E_{1,2}$, which are constant for smooth steady state solutions, are shown in Figure 7.

Exchange flow. The bottom topography, grid, and initial conditions are specified in the same way as in the previous example, but the layers are flowing in opposite directions, describing exchange flow between the reservoirs.

The boundary conditions are

$$\begin{aligned} (Q_1)_{in} &= 0.09282893, & (H_1)_{out} &= 0.1616669, \\ (Q_2)_{in} &= -0.09282893, & (H_2)_{out} &= 0.4311358, \end{aligned}$$

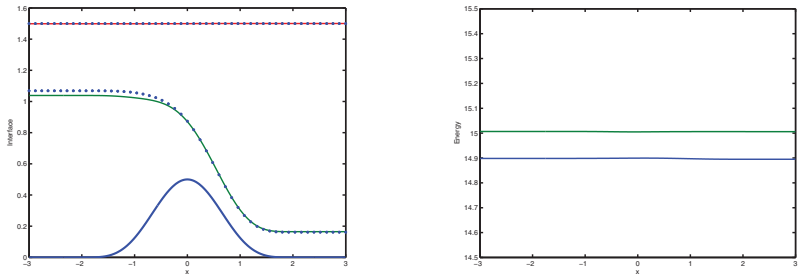

FIG. 7. *Smooth transcritical parallel flow. Interface and water surface (left), steady state flow energies $E_{1,2}$ (right).*

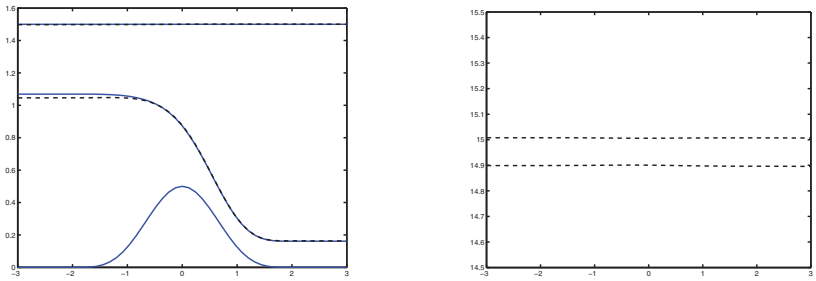

FIG. 8. *Smooth transcritical exchange flow. Interface and water surface (left) steady state flow energies $E_{1,2}$ (right).*

with the bottom layer flowing left to right and the top layer flowing right to left. The numerical solution shows very good agreement with the rigid-lid approximation; see Figure 8.

5.2.4. Hydraulic jump. In this example, the bottom elevation is removed, $B(x) = 0$, and the initial data is

$$\begin{aligned}(h_1, u_1, h_2, u_2)_L &= (0.9, 0.46, 1.1, -0.020255),\\ (h_1, u_1, h_2, u_2)_R &= (1, 0.414, 1, -0.0222280).\end{aligned}$$

These conditions correspond to a stationary jump satisfying the jump conditions (32a)–(32d) and assume the rigid-lid assumption with a total depth of $H_0 = 2$. The computed and exact solutions are shown in Figure 9 and correspond to a very long time integration ($T = 200$). The purpose here is to check the stability of the discontinuity and to allow all start-up errors to die out. We observe that the computed discontinuity is stable and that generally it is in very good agreement with the rigid-lid solution, with a small discrepancy in u_2 (equivalently F_2^2) primarily to the right of the jump. We note that this discrepancy, while to be expected, is quite small (of order $\mathcal{O}(10^{-4})$), corresponding to a relative difference of about 10%.

5.2.5. Transcritical flow with a hydraulic jump. The domain and bottom topography for this problem are the same as the transcritical example. The flow accelerates from sub- to supercritical as it goes over the bump but undergoes a hydraulic jump in order to match the boundary conditions on the right boundary. The exact (rigid-lid) steady state solution is piecewise smooth with a hydraulic jump to the right of the crest at $x = 0.48$. It is controlled by several constants whose definitions and

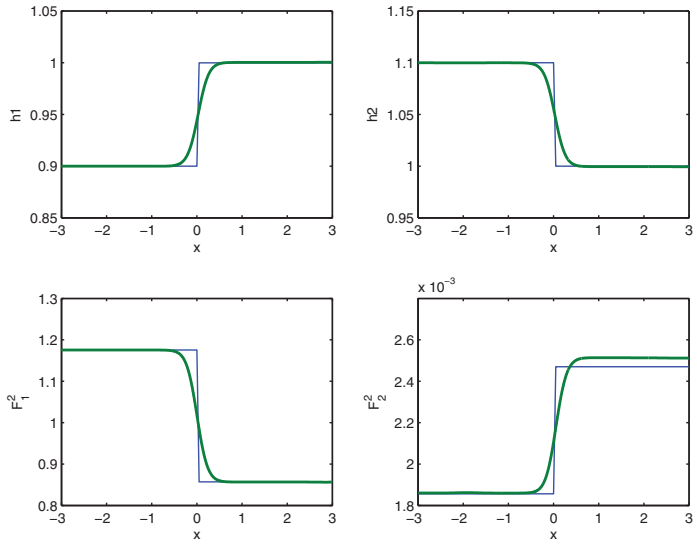

FIG. 9. *Hydraulic jump. Exact (with rigid-lid assumption) and computed solutions.*

notations are given in Appendix A. To the left of the jump, the steady state constants are $H_0 = 1.5$, $Q_r = 1$, and $\Delta E = 1.5$. The constants corresponding to the (smooth) solution to the right of the jump are determined by the jump conditions (32a)–(32d). The domain is discretized by 501 points, and the CFL number is 0.6. The exact (rigid-lid) solution values at both ends are then used as boundary conditions for solving (7); the flow rates $Q_{1,2}$ are specified at inflow and the layer depths $H_{1,2}$ at outflow:

$$\begin{aligned} (Q_1)_{in} &= 0.09282893, & (H_1)_{out} &= 0.9205217, \\ (Q_2)_{in} &= 0.09282893, & (H_2)_{out} &= 0.5794783. \end{aligned}$$

The computed solution as well as the exact rigid-lid solution are shown in Figure 10. The solutions are in good agreement, with some discrepancy in the subcritical (left) part of the flow and in the jump location. Again, we note that the comparison here is with the rigid-lid solution, and some discrepancy is to be expected. In particular, a small discrepancy in interface height may translate into larger error in velocity and seem to result in a discrepancy in jump location.

Appendix A. Exact steady state solutions. In this appendix, we briefly review the theory presented by Armi and Farmer [16, 17, 18] describing the hydraulics of two flowing layers. The theory is developed under the so-called *rigid-lid* assumption. Under the same assumption, we derive jump conditions valid across hydraulic jumps.

A.1. Nondimensionalizing. The layer *internal Froude number* is given by

$$F_i^2 = \frac{u_i^2}{g' h_i} = \frac{Q_i^2}{g' h_i^3}, \qquad i = 1, 2, \tag{27}$$

leading to the nondimensional relationship

$$\left(\frac{h_i}{H_0}\right)^3 = \frac{Q_i^2}{g' H_0^3} F_i^{-2},$$

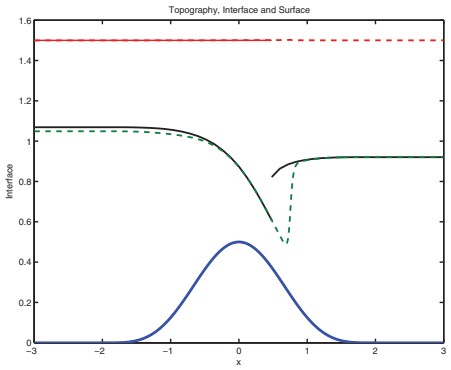

FIG. 10. *Transcritical flow with a hydraulic jump. Exact (rigid-lid, solid) and computed (dashed) solutions.*

where H_0 is a characteristic length (e.g., total flow depth). Introducing the nondimensional quantities $\tilde{h}_i = h_i/H_0$ and $\tilde{Q}_i^2 = Q_i^2/g'H_0^3$, one obtains the useful relationship

$$\tilde{h}_i = \tilde{Q}_i^{2/3} F_i^{-2/3}. \tag{28}$$

A.2. Rigid-lid assumption. This assumption somewhat simplifies the analysis and seems a reasonable assumption for many flows of interest. In the case of stratified flows, if the density difference between the layers is small, the external Froude number $U_m^2/g(h_1+h_2)$ is of order $\mathcal{O}(1-r)$ and the free surface remains leveled to order $\mathcal{O}(1-r)$ with $r = \rho_2/rho_1$ [16].

Taking H_0 to represent the total flow depth, the rigid-lid assumption reads

$$\tilde{h}_1 + \tilde{h}_2 + \tilde{B} = 1,$$

which may be expressed in terms of the Froude numbers using (28):

$$\tilde{Q}_1^{2/3} F_1^{-2/3} + \tilde{Q}_2^{2/3} F_2^{-2/3} + \tilde{B} = 1.$$

Upon further division by $\tilde{Q}_1$ and rearrangement of terms, one obtains

$$F_1^2 = \left\{ \left[\frac{\tilde{Q}_1}{(1-\tilde{B})^{3/2}} \right]^{-2/3} - Q_r^{2/3} (F_2^2)^{-1/3} \right\}^{-3}, \tag{29}$$

where $Q_r = \tilde{Q}_2/\tilde{Q}_1$. Equation (29) depends on the (normalized) bottom elevation $\tilde{B} = B(x)/H_0$ and will produce different curves for different elevations. We refer to the family of curves generated at different topography elevations as the *rigid-lid* curves.

A.3. Bernoulli's equation. Subtracting the energy equations in (6), one obtains

$$\frac{E_2 - E_1}{g'H_0} = \frac{1}{2}\frac{u_2^2}{g'H_0} - \frac{1}{2}\frac{u_1^2}{g'H_0} + \frac{h_2}{H_0}.$$

Expressing $u_i^2 = g'h_iF_i^2$ and denoting by $\Delta\tilde{E} = (E_2 - E_1)/(g'H_0)$ the nondimensional energy difference between the layers yields

$$\Delta\tilde{E} = \frac{1}{2}\tilde{Q}_2^{2/3} F_2^{4/3} - \frac{1}{2}\tilde{Q}_1^{2/3} F_1^{4/3} + \tilde{Q}_2^{2/3} F_2^{-2/3}.$$

Upon further division by $\tilde{Q}_2^{2/3}$ and rearrangement of terms one obtains

$$F_1^2 = Q_r \left[(F_2^2)^{2/3} + 2(F_2^2)^{-1/3} - 2\Delta E \right]^{3/2}, \tag{30}$$

with $\Delta E = \tilde{Q}_2^{-2/3} \Delta \tilde{E}$. Equation (30) does not depend on x and produces one curve for a given smooth steady flow, which we refer to as the *Bernoulli* curve.

The steady state solution at a given topography elevation is represented by the intersection of the Bernoulli curve with the corresponding rigid-lid curve and typically admits more than one solution. Boundary conditions determine which, if any, is the physically relevant solution.

A.4. Criticality condition. Smooth solutions for the single-layer shallow water system satisfy

$$B'(x) = \big(F^2 - 1\big) \frac{\partial h}{\partial x}$$

(here $F^2 = u^2/(gh)$), implying that at a crest ($B' = 0$) the solution is either symmetric, $\partial h/\partial x = 0$ (and can be either sub- or supercritical), or the flow is critical, that is, $F^2 = 1$. This condition is the shallow water analogue of the condition $M^2 = 1$ at the throat of a converging-diverging channel in Laval flow in hydrodynamics; here $M = |u|/c$ denotes the flow *Mach number* (see, for example, [26]). Laval flows are asymmetric flows that accelerate smoothly from sub- to supercritical and reach criticality at the throat of the channel (analogously at the topography crest for shallow water).

For the two-layer shallow water system, one can show in complete analogy that at a crest ($B' = 0$) the solution is either symmetric, $\frac{\partial}{\partial x}(\cdot) = 0$, or it reaches criticality, $G^2 = 1$, where G is the *composite Froude number* given by

$$G^2 = F_1^2 + F_2^2 - (1 - r) F_1^2 F_2^2,$$

where F_i denotes the internal Froude number given in (27). This condition is derived in Appendix B. $G^2 < 1$ (resp., $G^2 > 1$) represents subcritical (resp., supercritical) flow. For layers with $r \approx 1$, $G^2 \approx F_1^2 + F_2^2$ is considered a good approximation, which yields the following approximate equality, hereafter refered to as the *criticality* condition:

$$F_1^2 = 1 - F_2^2. \tag{31}$$

The three relevant curves for determining smooth steady state solutions for two-layer shallow water flows are illustrated in Figure 11. We note one Bernoulli curve in blue and two rigid-lid curves in red, one corresponding to the crest and one to the foot of the topography hump, marking the boundaries that enclose the family of rigid-lid curves for intermediate values of topography elevation. One such intermediate curve is marked in black. The criticality condition is marked by the green curve, below which the flow is subcritical and above which it is supercritical.

We make the following remarks:

(i) Asymmetric steady flows, namely, flows which accelerate smoothly from sub- to supercritical, are delicate to compute as the solution admits multiple roots. As in the single-layer shallow water case, the solution at the crest itself is a double root and splits into two nearby roots off the crest, one corresponding

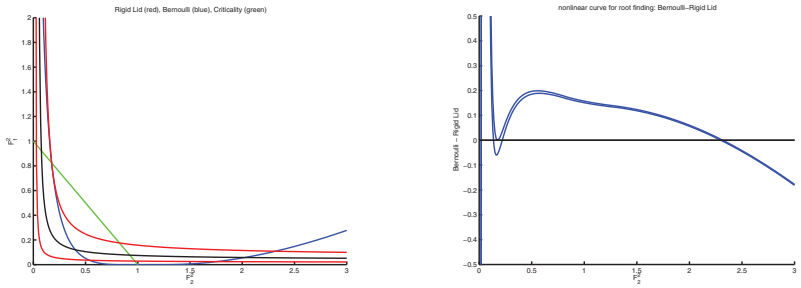

FIG. 11. *Smooth steady state solutions. (Left) Bernoulli curve (blue), rigid-lid curves corresponding to the crest and foot of topography hump (red), and the criticality condition (green); (right) solution root finding curve at the crest (double root) and slightly below the crest.*

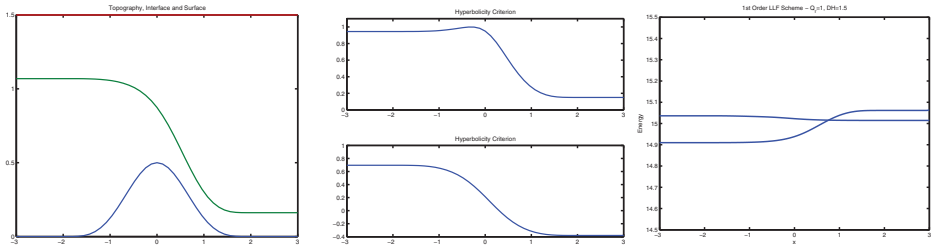

FIG. 12. *(Left) Steady state solution of smoothly accelerating flow from sub- to supercritical flow, reaching criticality at the crest; (middle) hyperbolicity condition for steady state parallel flow (top) and exchange flow (bottom); (right) flow energies* $E_{1,2}$. *Variation in energies indicate that the rigid-lid solution is only an approximate steady state of* (1).

to subcritical flow and one corresponding to supercritical flow (accordingly, these roots are below and above the (green) criticality curve, respectively). This is illustrated in Figure 11. The corresponding asymmetric smooth steady solution is shown in Figure 12.

(ii) We note that the steady state solution depends on Q_r^2 and therefore does not distinguish between layers that are flowing in the same direction or in opposite directions; the latter is referred to in the hydraulics literature as *exchange flow*. Exchange flow is more likely to develop shear instability and accordingly violate the approximate hyperbolicity condition (5). The hyperbolicity condition for the smooth steady solution in Figure 12 is also plotted and establishes that exchange flow for these flow parameters violates the approximate hyperbolicity condition (reflected by the occurrence of negative values).

(iii) While it is tempting to use the approximate hyperbolicity condition (5) as an indication for the hyperbolicity of the underlying flow, we note that condition (5) may be violated while the underlying flow is time-hyperbolic (i.e., exact eigenvalues are real). This is the case for the example shown in Figure 12.

(iv) The above exact solution uses the rigid-lid assumption and is therefore only an approximate steady solution for system (1). A measure for how good this approximation is can be obtained by computing the quantities $Q_{1,2}$ and $E_{1,2}$, which should be constant, and observing their variation over the domain. Figure 12 illustrates the variations in flow constants resulting from the rigid-lid assumption.

A.5. Hydraulic jumps. System (1) is in nonconservation form, which makes the definition of discontinuous solutions more subtle. Underlying the nonconservation form is, however, an essential conservation of mass in the individual layers and of the *total* momentum, that is, the sum of the momenta in the layers. For flows where the total water depth is nearly constant, the rigid-lid assumption may be used as a fourth condition to enable formulating jump conditions across hydraulic jumps.

We assume that a left state W_L is given and seek a right state W_R that satisfies

$$\big[h_1 u_1\big] = 0, \tag{32a}$$

$$\big[h_2 u_2\big] = 0, \tag{32b}$$

$$\Big[h_1 u_1^2 + r h_2 u_2^2 + \frac{g}{2}(h_1^2 + 2r h_1 h_2 + r h_2^2)\Big] = 0, \tag{32c}$$

$$\big[B + h_1 + h_2\big] = \big[h_1 + h_2\big] = 0, \tag{32d}$$

where $[\cdot] = (\cdot)_L - (\cdot)_R$ denotes the jump across the discontinuity and the fourth condition is the rigid-lid assumption. Setting $Q_i = h_i u_i$, (32c) becomes

$$Q_1^2 \left(\frac{1}{h_1^L} - \frac{1}{h_1^R}\right) + r Q_2^2 \left(\frac{1}{h_2^L} - \frac{1}{h_2^R}\right) + \frac{g}{2}\big[h_1^2 + 2r h_1 h_2 + r h_2^2\big] = 0.$$

We note that $h_1^2 + 2r h_1 h_2 + r h_2^2 = (1-r)h_1^2 + r(h_1 + h_2)^2$ and that the rigid-lid assumption implies that $\big[r(h_1 + h_2)^2\big] = 0$. The above equation reduces to

$$Q_1^2 \, \frac{h_1^R - h_1^L}{h_1^L h_1^R} + r Q_2^2 \, \frac{h_2^R - h_2^L}{h_2^L h_2^R} + \frac{g}{2}\big(1-r\big)\Big(h_1^L - h_1^R\Big)\Big(h_1^L + h_1^R\Big) = 0.$$

Finally, we note that the rigid-lid assumption implies $h_1^R - h_1^L = -(h_2^R - h_2^L)$, and a common factor can be eliminated from the above equation to give

$$Q_1^2 \, \frac{1}{h_1^L h_1^R} - Q_2^2 \, \frac{r}{h_2^L h_2^R} - \frac{g}{2}\big(1-r\big)\big(h_1^L + h_1^R\big) = 0.$$

Denoting by $x = h_1^R$ and $\theta = h_1^L + h_2^L = h_1^R + h_2^R$, we have $h_2^R = \theta - x$ and the jump condition are expressed as the root of a cubic equation in x given by

$$\frac{Q_1^2}{h_1^L} \, \frac{1}{x} - \frac{Q_2^2}{h_2^L} \, \frac{r}{\theta - x} - \frac{g}{2}\big(1-r\big)\big(h_1^L + x\big) = 0. \tag{33}$$

The remaining state variables of W_R are then computed from (32). We close by remarking that the admissibility of the resulting jump should be verified with respect to an "entropy-like" condition. This is a somewhat vague statement, but we believe some version of it should hold. For example, admissible steady shocks in fluid dynamics must be supersonic ($M^2 > 1$) ahead of the shock and subsonic ($M^2 < 1$) behind it. In shallow water flows, it is possible that an analogous admissibility criterion holds for the composite Froude number G^2, although we are not aware of an established connection between this statement and the entropy condition.

Appendix B. Criticality condition. We consider the steady state version of (1), written in terms of the primitive variables h_1, h_2, u_1, and u_2:

$$u_1 \frac{\partial h_1}{\partial x} + h_1 \frac{\partial u_1}{\partial x} = 0, \tag{34a}$$

$$u_1\frac{\partial u_1}{\partial x}+g\frac{\partial h_1}{\partial x}+rg\frac{\partial h_2}{\partial x}+g\frac{dB}{dx}=0, \tag{34b}$$

$$u_2\frac{\partial h_2}{\partial x}+h_2\frac{\partial u_2}{\partial x}=0, \tag{34c}$$

$$u_2\frac{\partial u_2}{\partial x}+g\frac{\partial h_2}{\partial x}+g\frac{\partial h_1}{\partial x}+g\frac{dB}{dx}=0 \tag{34d}$$

(here g' continues to denote $(1-r)g$). From the definition of the (internal) Froude number, we get

$$u_i^2=g'h_iF_i^2$$

so that

$$-\frac{h_{i,x}}{h_i}+2\frac{u_{i,x}}{u_i}=2\frac{F_{i,x}}{F_i} \tag{35}$$

(here $(\ )_{i,x}=\frac{\partial}{\partial x}(\ )_i$). Combined with (34a) and (34c), we get for steady state solutions

$$3\frac{u_{i,x}}{u_i}=2\frac{F_{i,x}}{F_i},$$

which we can use to eliminate u_i in (34b) and (34d):

$$\begin{aligned}\tfrac{2}{3}g'h_1F_1\frac{\partial F_1}{\partial x}+g\frac{\partial h_1}{\partial x}+rg\frac{\partial h_2}{\partial x}+g\frac{dB}{dx}=0,\\ \tfrac{2}{3}g'h_2F_2\frac{\partial F_2}{\partial x}+g\frac{\partial h_1}{\partial x}+g\frac{\partial h_2}{\partial x}+g\frac{dB}{dx}=0.\end{aligned} \tag{36}$$

Using (27) we write

$$Q_i^2=g'h_i^3F_i^2. \tag{37}$$

Substituting (37) into (36), we find

$$\begin{aligned}&\left(g'F_1^{1/3}-gF_1^{-5/3}\right)Q_1^{2/3}\frac{\partial F_1}{\partial x}-grF_2^{-5/3}Q_2^{2/3}\frac{\partial F_2}{\partial x}+\frac{3}{2}g(g')^{1/3}\frac{dB}{dx}=0,\\ &-gF_1^{-5/3}Q_1^{2/3}\frac{\partial F_1}{\partial x}+\left(g'F_2^{1/3}-gF_2^{-5/3}\right)Q_2^{2/3}\frac{\partial F_2}{\partial x}+\frac{3}{2}g(g')^{1/3}\frac{dB}{dx}=0.\end{aligned} \tag{38}$$

At the crest, $\frac{dB}{dx}=0$. With respect to the variables $Q_i^{2/3}\frac{\partial F_i}{\partial x}$, system (38) may be satisfied trivially if $\frac{\partial}{\partial x}(\ )=0$, yielding the symmetric solution. For a nontrivial solution to exist, the determinant of the coefficient matrix

$$\begin{vmatrix} g'F_1^{1/3}-gF_1^{-5/3} & -grF_2^{-5/3}\\ -gF_1^{-5/3} & g'F_2^{1/3}-gF_2^{-5/3}\end{vmatrix}$$

must vanish. That is,

$$\left(g'F_1^2-g\right)\left(g'F_2^2-g\right)-g^2r=0,$$

which after simplification gives the criticality condition (31)

$$F_1^2+F_2^2-(1-r)F_1^2F_2^2=1. \tag{39}$$

Appendix C. Chapman–Enskog expansion of (12). We start from (7):

$$\frac{\partial}{\partial t}(\rho_1 h_1) + \frac{\partial}{\partial x}(\rho_1 h_1 u_1) = 0,$$
$$\frac{\partial}{\partial t}(\rho_1 h_1 u_1) + \frac{\partial}{\partial x}\left(\rho_1 h_1 u_1^2 + \rho_1 g \frac{h_1^2}{2} + \boxed{\rho_2 g h_1 h_2^{'}}\right) = \boxed{\rho_2 g h_2 \frac{\partial h_1^{'}}{\partial x}} - \rho_1 g h_1 B'(x),$$
$$\frac{\partial}{\partial t}(\rho_2 h_2) + \frac{\partial}{\partial x}(\rho_2 h_2 u_2) = 0,$$
$$\frac{\partial}{\partial t}(\rho_2 h_2 u_2) + \frac{\partial}{\partial x}\left(\rho_2 h_2 u_2^2 + \rho_2 g \frac{h_2^2}{2}\right) = -\boxed{\rho_2 g h_2 \frac{\partial h_1^{'}}{\partial x}} - \rho_2 g h_2 B'(x),$$
$$\frac{\partial}{\partial t} h_1^{'} + U_1^* \frac{\partial}{\partial x} h_1^{'} = \frac{h_1^{'} - h_1}{\epsilon},$$
$$\frac{\partial}{\partial t} h_2^{'} + U_2^* \frac{\partial}{\partial x} h_2^{'} = \frac{h_2^{'} - h_2}{\epsilon},$$

which is rewritten with clear notations as

$$\frac{\partial U}{\partial t} + \frac{\partial}{\partial x} G(U) + \begin{pmatrix} 0 \\ \dfrac{\partial}{\partial x}\left(\rho_2 g h_1 h_2'\right) - \rho_2 g h_2 \dfrac{\partial h_1'}{\partial x} \\ 0 \\ -\rho_2 g h_2 \dfrac{\partial h_1'}{\partial x} \end{pmatrix} = S_U, \tag{40a}$$

$$\begin{aligned} &\frac{\partial}{\partial t} h_1^{'} + U_1^* \frac{\partial}{\partial x} h_1^{'} = \frac{h_1^{'} - h_1}{\epsilon}, \\ &\frac{\partial}{\partial t} h_2^{'} + U_2^* \frac{\partial}{\partial x} h_2^{'} = \frac{h_2^{'} - h_2}{\epsilon}. \end{aligned} \tag{40b}$$

Formally, we write

$$h_1' = h_1 + \epsilon \Theta_1, \qquad h_2' = h_2 + \epsilon \Theta_2.$$

Using (40b), we see that

$$\Theta_1 = \frac{\partial}{\partial t} h_1^{'} + U_1^* \frac{\partial}{\partial x} h_1^{'},$$
$$\Theta_2 = \frac{\partial}{\partial t} h_2^{'} + U_2^* \frac{\partial}{\partial x} h_2^{'}.$$

If we set $U_1^* = u_1$ and $U_2^* = u_2$, we can use the system (40a) and get

$$\Theta_1 = -h_1 \frac{\partial u_1}{\partial x} + \epsilon\left(\frac{\partial \Theta_1}{\partial t} + u_1 \frac{\partial \Theta_1}{\partial x}\right),$$
$$\Theta_2 = -h_2 \frac{\partial u_2}{\partial x} + \epsilon\left(\frac{\partial \Theta_2}{\partial t} + u_2 \frac{\partial \Theta_2}{\partial x}\right).$$

Then we consider the term

$$\begin{aligned} \frac{\partial}{\partial x}\left(\rho_2 g h_1 h_2'\right) - \rho_2 g h_2 \frac{\partial h_1'}{\partial x} &= \rho_2 g \left(h_2' \frac{\partial}{\partial x}(h_1 - h_1') + h_1 \frac{\partial h_2'}{\partial x}\right) \\ &= \rho_2 g \left(\epsilon h_2 \frac{\partial \Theta_1}{\partial x} + h_1 \frac{\partial h_2}{\partial x} + \epsilon h_1 \frac{\partial \Theta_1}{\partial 2}\right) \\ &= \rho_2 g h_1 \frac{\partial h_2}{\partial x} - \epsilon \rho_2 g h_2 h_1 \frac{\partial u_1}{\partial x} + O(\epsilon^2) \end{aligned}$$

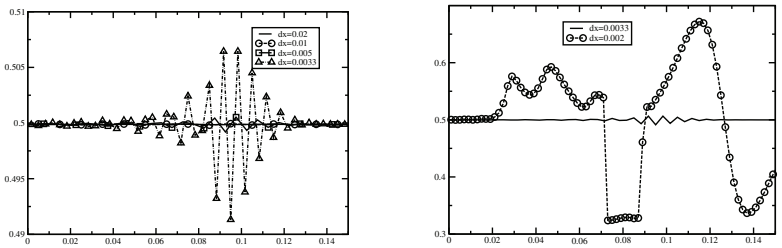

(a) (b)

FIG. 13. *Results with the relaxed model,* $\epsilon = 0.000001$*, for* (a) $N = 100, 200, 400,$ *and* 600 *points and* (b) $N = 600$ *and* 1000 *points. The instability depends on the number of mesh points.*

and the term

$$-\rho_2 g h_2 \frac{\partial h_1'}{\partial x} = -\rho_2 g h_2 \frac{\partial h_1}{\partial x} - \epsilon g \rho_2 h_2 \frac{\partial \Theta_2}{\partial x}$$
$$= -\rho_2 g h_2 \frac{\partial h_1}{\partial x} + \epsilon g \rho_2 h_2^2 \frac{\partial u_2}{\partial x} + O(\epsilon^2).$$

After projection, the relaxation model writes

$$\frac{\partial U}{\partial t} + \frac{\partial G}{\partial x} = S_U(U) + \epsilon \frac{\partial}{\partial x}\left(D\left(U, \frac{\partial U}{\partial x}\right)\right),$$

where

$$D\left(U, \frac{\partial U}{\partial x}\right) = \begin{pmatrix} 0 & 0 & 0 & 0 \\ 0 & \rho_2 g h_1 h_2 \dfrac{\partial u_1}{\partial x} & 0 & 0 \\ 0 & 0 & 0 & 0 \\ 0 & 0 & 0 & g\rho_2 h_2^2 \dfrac{\partial u_2}{\partial x} \end{pmatrix}.$$

The operator $D(U, \frac{\partial U}{\partial x})$ is not positive in general.

Appendix D. Relaxation and numerical parameters—numerical study. We conducted a series of numerical experiments to investigate the intricate interplay between the relaxation parameter ϵ and numerical parameters such as grid size and CFL number. The study indicates that the Chapman–Enskog expansion provides only part of the stability picture, and small parameters such as the grid size certainly play an important role in the final stability account.

In order to illustrate this point, we study the behavior of the relaxation system (7) for a finite value of ϵ. We integrate the first four equations using the Roe scheme as described above. The last two are integrated using an explicit Roe discretization of the $U_i^* \frac{\partial}{\partial x} h_i'$ terms and an implicit approximation of the source term, where h_i is evaluated at t_{n+1}, which is already available. The resulting scheme is implicit in time and enables us to run the model with time steps independent of ϵ.

We have chosen a small value of ϵ, $\epsilon = 0.000001$, and computed, for the same physical time as in Figure 3, the solution for 100, 200, 400, 600, and 1000 grid points. The results are displayed in Figure 13. The instability clearly shows dependence on the number of mesh points.

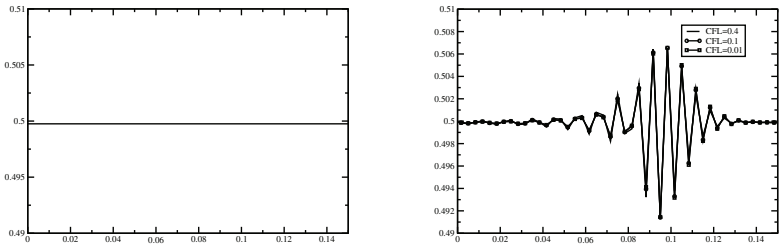

(a) (b)

FIG. 14. *Results with* (a) *the model without relaxation and* (b) *the relaxation model for* $\epsilon = 0.000001$. *The original model is stable; the instability of the relaxation model is CFL-independent.*

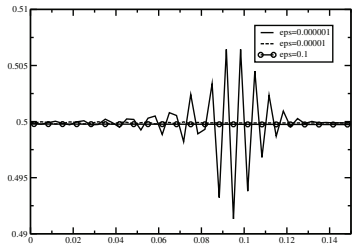

FIG. 15. *Results with* $N = 600$ *grid points and different values of* ϵ. *The instability is* ϵ*–dependent.*

For comparison, we have computed the solution for the original system (1) using the scheme (25)–(26) and for the relaxation system (7) with $\epsilon = 0.000001$ for various CFL numbers, using $N = 600$ points. The results are shown in Figure 14. The original model apears to be stable, and the instability of the relaxation model appears to be independent of the CFL number.

In a last series of experiments, we fix the number of grid points ($N = 600$ again) and let ϵ vary from 0.000001 to 0.1. The results are shown in Figure 15 and appear to be very dependent on ϵ. We conclude from this quick study that the instability implied by the Chapman–Enskog expansion provides only a crude indication of the stability of the numerical solutions, an indication which does not give a complete account of the intricate interplay between the relaxation parameter and other small numerical parameters.

REFERENCES

[1] G. DALMASO, P.G. LE FLOCH, AND F. MURAT, *Definition and weak stability of nonconservative products*, J. Math. Pures Appl. 9, 74 (1995), pp. 483–548.

[2] P.G. LE FLOCH, *Graph solutions of nonlinear hyperbolic systems*, J. Hyperbolic Differ. Equ., 2 (2004), pp. 643–689.

[3] P.-A. RAVIART AND L. SAINSAULIEU, *A nonconservative hyperbolic system modeling spray dynamics.* I. *Solution of the Riemann problem*, Math. Models Methods Appl. Sci., 5 (1995), pp. 297–333.

[4] I. TOUMI, *A weak formulation of Roe's approximate Riemann solver*, J. Comput. Phys., 102 (1992), pp. 360–373.

[5] M.J. CASTRO, J. MACIAS, AND C. PARES, *A Q-scheme for a class of systems of coupled conservation laws with source terms. Application to a two-layer* 1*-d shallow water system*, M2AN Math. Model. Numer. Anal., 35 (2001), pp. 107–127.

[6] C. PARES AND M. CASTRO, *On the well-balance property of Roe's method for nonconservative hyperbolic systems. Applications to shallow-water systems*, M2AN Math. Model. Numer. Anal., 38 (2004), pp. 821–852.

[7] M.J. Castro, J.A. Garcia-Rodriguez, J.M. Gonzalez-Vida, J. Macias, C. Pares, and M.E. Vazquez-Cendon, *Numerical simulation of two-layer shallow water flows through channels with irregular geometry*, J. Comput. Phys., 195 (2004), pp. 202–235.
[8] M.J. Castro Díaz, T. Chacón Rebollo, E.D. Fernández-Nieto, and C. Parés, *On well-balanced finite volume methods for nonconservative nonhomogeneous hyperbolic systems*, SIAM J. Sci. Comput., 29 (2007), pp. 1093–1126.
[9] E. Audusse, *A multilayer Saint-Venant model*, Discrete Contin. Dyn. Syst., Ser. B, 5 (2005), pp. 189–214.
[10] E. Audusse and M.O. Bristeau, *Finite-volume solvers for a multilayer Saint-Venant system*, Int. J. Appl. Math. Comput. Sci., 17 (2007), pp. 311–320.
[11] C. Parés, *Numerical methods for nonconservative hyperbolic systems: A theoretical framework*, SIAM J. Numer. Anal., 44 (2006), pp. 300–321.
[12] F. Bouchut, *Nonlinear Stability of Finite Volume Methods for Hyperbolic Conservation Laws and Well-balanced Schemes for Sources*, Birkhäuser, Basel, Switzerland, Berlin, 2004.
[13] J.B. Schijf and J.C. Schonfeld, *Theoretical considerations on the motion of salt and fresh water*, in Proceedings of the Minnesota International Hydraulics Convention, Joint meeting International Association Hydraulic Research and Hydraulic Division American Society Civil Engineers, 1953, pp. 321–333.
[14] R.R. Long, *Long waves in a two-fluid system*, J. Met., 13 (1956), pp. 70–74.
[15] E. Godlewski and P.-A. Raviart, *Numerical Approximation of Hyperbolic Systems of Conservation Laws*, Appl. Math. Sci. 118, Springer-Verlag, New York, 1996.
[16] L. Armi, *The hydraulics of two flowing layers with different densities*, J. Fluid Mech., 163 (1986), pp. 27–60.
[17] L. Armi and D.M. Farmer, *Maximal two-layer exchange through a contraction with barotropic net flow*, J. Fluid Mech., 186 (1986), pp. 27–51.
[18] D.M. Farmer and L. Armi, *Maximal two-layer exchange over a sill and through the combination of sill and a contraction with barotropic flow*, J. Fluid Mech., 164 (1986), pp. 53–76.
[19] A. Murrone and H. Guillard, *A five equation reduced model for compressible two phase flow problems*, J. Comput. Phys., 202 (2005), pp. 664–698.
[20] S. Chapman and T.G. Cowling, *The Mathematical Theory of Nonuniform Gases*, 3rd ed., Cambridge University Press, Cambridge, 1970.
[21] G.-Q. Chen, D. Levermore, and T.-P. Liu, *Hyperbolic conservation laws with stiff relaxation terms and entropy*, Comm. Pure Appl. Math., 47 (1994), pp. 787–830.
[22] S. Jin and Z. Xin, *The relaxation scheme for systems of conservation laws in arbitrary space dimensions*, Comm. Pure Appl. Math., 48 (1995), pp. 235–276.
[23] R. Natalini, *Recent results on hyperbolic relaxation problems*, in Analysis of Systems of Conservation Laws (Aachen, 1997), Chapman & Hall/CRC Monogr. Surv. Pure Appl. Math. 99, Chapman & Hall/CRC, Boca Raton, FL, 1999, pp. 128–198.
[24] P.L. Roe, *Approximate Riemann solvers, parameter vectors and difference schemes*, J. Comput. Phys., 43 (1981), pp. 357–372.
[25] P.L. Roe, *Upwind differencing schemes for hyperbolic conservation laws with source terms*, in Nonlinear Hyperbolic Problems, Springer-Verlag, Berlin, Heidelberg, in Lect. Notes in Math. 1270, 1987, pp. 41–51.
[26] R. Courant and K.O. Friedrichs, *Supersonic Flow and Shock Waves*, Appl. Math. Sci. 21, Springer-Verlag, New York, 1948.